

# Fock-space relativistic coupled-cluster calculation of hyperfine induced $^1S_0 \rightarrow ^3P_0^o$ clock transition in $\text{Al}^+$

Ravi Kumar,<sup>1</sup> S. Chattopadhyay,<sup>2</sup> D. Angom,<sup>3</sup> and B. K. Mani<sup>1,\*</sup>

<sup>1</sup>*Department of Physics, Indian Institute of Technology, Hauz Khas, New Delhi 110016, India*

<sup>2</sup>*Department of Physics, Kansas State University, Manhattan, Kansas 66506, USA*

<sup>3</sup>*Physical Research Laboratory, Ahmedabad - 380009, Gujarat, India*

We have developed an all-particle Fock-space relativistic coupled-cluster method to accurately calculate the properties of two-valence atoms and ions. Using the method we have calculated the properties associated with  $^1S_0 - ^3P_0^o$  clock transition in  $\text{Al}^+$ . Our calculated life time of  $^3P_0^o$  metastable state,  $20.20 \pm 0.68$  s, is in excellent agreement with the experimental value,  $20.60 \pm 1.4$  s, from Rosenband *et al.*, Phys. Rev. Lett. **98**, 220801 (2007). From our calculations we also find that the contributions from the triple excitations and Breit+QED corrections are critical to obtain the accurate clock properties in  $\text{Al}^+$ .

## I. INTRODUCTION

The atomic clocks as frequency standard provide a roadmap to study several fundamental as well as technological applications. Some examples are the variation of the fundamental constants, probing physics beyond the standard model of particle physics, navigation systems and the basis for the redefinition of the second [1–4]. The recent frequency standard experiments [5–9] in optical domain have reported  $^1S_0 - ^3P_0^o$  transition in  $\text{Al}^+$  as one of the most accurate clock transitions. Though the  $^1S_0 - ^3P_0^o$  transition is highly forbidden based on the selection rule of the total electronic angular momentum  $J$ , it is possible through hyperfine mixing of the  $^3P_0^o$  state with  $^3P_1^o$  and  $^1P_1^o$  states. The life time of the  $^3P_0^o$  metastable clock state was measured with high accuracy by Rosenband and collaborators [5] using the quantum logic spectroscopy technique. The reasons supporting the choice for this transition as clock transition are low sensitivity to electromagnetic fields, narrow natural linewidth and small room temperature black-body radiation shift. The latter is due to small difference between the polarizabilities of  $^1S_0$  and  $^3P_0^o$  states [10, 11]. A recent work reported fractional frequency uncertainty of a  $^1S_0 - ^3P_0^o$  transition based  $\text{Al}^+$  clock as  $9.4 \times 10^{-19}$  [8]. And, this, perhaps, is the most precise atomic clock in existence today.

Despite the important applications of the  $^1S_0 - ^3P_0^o$  hyperfine induced electric dipole transition (E1HFS), and several experimental investigations in progress, very little theoretical data on the associated properties is available. For example, there are only two results on the life time of  $^3P_0^o$  metastable clock state [12, 13], and both are based on the method of multiconfiguration Dirac-Fock. To the best of our knowledge, there are no theoretical results using the accurate many-body methods like relativistic coupled-cluster (RCC). It is to be emphasized that the RCC is considered to be one of the most accurate many-body theories for properties calculations of atoms and ions. It accounts for the electron correlation effects to all-orders of residual Coulomb interaction, and has been employed to calculate a plethora of properties accurately

in several closed-shell and one-valence atoms and ions [14–17]. The implementation of RCC for structure and properties calculations of two-valence atomic systems is, however, limited to few studies [18–20]. The reason, perhaps, is the complications associated with its implementation for two-valence systems. To be more precise, there are three main hurdles. First, due to the multireference nature of the configuration space, the model wave function is not well defined. This needs a special treatment through the diagonalization of the effective Hamiltonian matrix. Second, the atomic states are the eigen states of the total angular momentum, which leads to a complication in the angular factors associated with antisymmetrized many-electron states. And third, divergence due to *intruder* states.

It can thus be surmised that there is a clear research gap in terms of the scarcity of accurate theoretical data on  $^1S_0 - ^3P_0^o$  E1HFS properties. The aim of this work is to fill this research gap. Our objectives of this paper are: to develop a Fock space relativistic coupled-cluster (FSRCC) based method for structure and properties calculations of two-valence atoms or ions; using the method, compute the properties associated with  $^1S_0 - ^3P_0^o$  E1HFS such as the excitation energies, hyperfine structure constants, oscillator strengths and more importantly the life time of the  $^3P_0^o$  state; and finally, examine in the detail the contributions from the dominant triples, Breit interaction and QED corrections to these properties.

The remaining part of the paper is organized as follows. In Sec. II we provide an overview of the FSRCC for two-valence systems. In Sec. III we discuss properties calculation using two-valence FSRCC, where we also provide the properties diagrams. In Sec. IV we provide the details of the basis functions, nuclear potential, etc., used in the calculations. The results obtained from our calculations are analyzed and discussed in Sec. V. The theoretical uncertainty in our calculated results is discussed in Sec. VI of the paper. Unless stated otherwise, all the results and equations presented in this paper are in atomic units ( $\hbar = m_e = e = 1/4\pi\epsilon_0 = 1$ ).

## II. FSRCC FOR TWO-VALENCE

The Dirac-Coulomb-Breit no-virtual-pair Hamiltonian,  $H^{\text{DCB}}$ , is considered as the zeroth order Hamiltonian. It ac-

\* [bkmani@physics.iitd.ac.in](mailto:bkmani@physics.iitd.ac.in)

counts for the relativistic effects and provide an appropriate description of the high- $Z$  atoms or ions. For an  $N$ -electron atom or ion

$$H^{\text{DCB}} = \sum_{i=1}^N [c\alpha_i \cdot \mathbf{p}_i + (\beta_i - 1)c^2 - V_N(r_i)] + \sum_{i < j} \left[ \frac{1}{r_{ij}} + g^B(r_{ij}) \right], \quad (1)$$

where  $\alpha$  and  $\beta$  are the Dirac matrices, and  $V_N(r_i)$  is the nuclear potential. The ill effects of negative-energy continuum states are removed by employing the kinetically balanced finite Gaussian basis [21, 22]. The last two terms,  $1/r_{ij}$  and  $g^B(r_{ij})$  are the Coulomb and Breit interactions, respectively. The Breit interaction, which represents the inter-electron magnetic interactions, is

$$g^B(r_{12}) = -\frac{1}{2r_{12}} \left[ \alpha_1 \cdot \alpha_2 + \frac{(\alpha_1 \cdot \mathbf{r}_{12})(\alpha_2 \cdot \mathbf{r}_{12})}{r_{12}^2} \right]. \quad (2)$$

In the FSRCC for two-valence atoms or ions,  $H^{\text{DCB}}$  can be partitioned as: (a)  $H_{0v}^{\text{DCB}}$ , the part which spans the Hilbert space of the closed-shell electrons; (b)  $H_{1v}^{\text{DCB}}$ , which spans the Hilbert space of closed-shell and an additional electron; and (c)  $H_{2v}^{\text{DCB}}$ , the Hamiltonian spanning the Hilbert space of two valence electrons. One of the key advantages of this strategy is the sector wise separation of the cluster operators [23].

Following this strategy of sector wise separation of the total Hilbert space of the two-valence configurations, we can write the eigenvalue equation for closed-shell sector as

$$H_{0v}^{\text{DCB}}|\Psi_0\rangle = E_0|\Psi_0\rangle, \quad (3)$$

where  $|\Psi_0\rangle$  is the exact atomic state and  $E_0$  is the exact energy of the closed-shell. In the RCC method

$$|\Psi_0\rangle = e^T|\Phi_0\rangle, \quad (4)$$

where  $T$  is the closed-shell cluster operator and  $|\Phi_0\rangle$  is the closed-shell Dirac-Fock reference state. For a two-valence system with  $N$  electrons

$$T = \sum_{i=1}^{N-2} T_i. \quad (5)$$

Among cluster operators the single and double excitations clusters  $T_1$  and  $T_2$ , respectively, subsume most of the electron correlation effects. Therefore, we can approximate  $T = T_1 + T_2$ , and this is referred to as the coupled-cluster with singles and doubles (CCSD) approximation. The dominant contributions from the triple excitations are, however, also included in the present work using the perturbative triples approach. The details of the method are discussed in the latter part of the paper. In the second quantized notations

$$T_1 = \sum_{ap} t_a^p a_p^\dagger a_a, \quad (6a)$$

$$T_2 = \frac{1}{2!} \sum_{abpq} t_{ab}^{pq} a_p^\dagger a_q^\dagger a_b a_a. \quad (6b)$$

The indices  $abc\dots$  ( $pqr\dots$ ) represent the core (the virtual) states, and  $t_a^p$  and  $t_{ab}^{pq}$  are the corresponding amplitudes. The operators  $T_1$  and  $T_2$  acts on the reference state  $|\Phi_0\rangle$  to produce single and double replacements of electrons. And, the cluster amplitudes are obtained after solving the coupled nonlinear equations

$$\langle \Phi_a^p | \bar{H}_N | \Phi_0 \rangle = 0, \quad (7a)$$

$$\langle \Phi_{ab}^{pq} | \bar{H}_N | \Phi_0 \rangle = 0, \quad (7b)$$

where  $\bar{H}_N = e^{-T^{(0)}} H_N e^{T^{(0)}}$  is the similarity transformed or dressed Hamiltonian.

Like in the closed-shell sector, the eigenvalue equation for the one-valence sector is

$$H_{1v}^{\text{DCB}}|\Psi_v\rangle = E_v|\Psi_v\rangle, \quad (8)$$

where  $|\Psi_v\rangle$  is the exact atomic state and  $E_v$  is the corresponding energy. In RCC

$$|\Psi_v\rangle = e^{T+S}|\Phi_v\rangle = e^T(1+S)|\Phi_v\rangle. \quad (9)$$

Here,  $|\Phi_v\rangle$  is the one-valence Dirac-Fock reference state obtained by adding an electron to the closed-shell reference state,  $a_v^\dagger|\Phi_0\rangle$ . The operator  $S$  is referred to as the CC operator for one-valence sector. For a two-valence atom with  $N$ -electrons,  $S = \sum_{i=1}^{N-1} S_i$  and, similar to  $T$ , within CCSD approximation  $S = S_1 + S_2$ . The second quantized representation of these operators are

$$S_1 = \sum_p s_v^p a_p^\dagger a_v, \quad (10a)$$

$$S_2 = \sum_{apq} s_{va}^{pq} a_p^\dagger a_q^\dagger a_a a_v, \quad (10b)$$

and are solutions of the set of linear coupled equations

$$\langle \Phi_v^p | \bar{H}_N + \{\bar{H}_N S\} | \Phi_v \rangle = E_v^{\text{att}} \langle \Phi_v^p | S_1 | \Phi_v \rangle, \quad (11a)$$

$$\langle \Phi_{va}^{pq} | \bar{H}_N + \{\bar{H}_N S\} | \Phi_v \rangle = E_v^{\text{att}} \langle \Phi_{va}^{pq} | S_2 | \Phi_v \rangle. \quad (11b)$$

Here,  $E_v^{\text{att}}$  is the attachment energy of an electron to the  $v$ -shell. It is defined as  $E_v^{\text{att}} = E_v - E_0$ , the difference between the correlated energy of  $(n-2)$ -electron (closed-shell) sector and the  $(n-1)$ -electron (one-valence) sector. Alternatively, it is

$$E_v^{\text{att}} = \epsilon_v + \Delta E_v^{\text{att}}, \quad (12)$$

where  $\epsilon_v$  is the Dirac-Fock energy of the valence electron in  $|\phi_v\rangle$  and  $\Delta E_v^{\text{att}}$  is the difference of the correlation energy of closed-shell from the one-valence sector,  $\Delta E_v^{\text{corr}} - \Delta E_0^{\text{corr}}$ .

Like in the case of closed-shell and one-valence sectors, the eigenvalue equation for two-valence sector is

$$H_{2v}^{\text{DCB}}|\Psi_{vw}\rangle = E_{vw}|\Psi_{vw}\rangle, \quad (13)$$

where  $|\Psi_{vw}\rangle$  is the two-valence exact atomic state and  $E_{vw}$  is the corresponding energy. In RCC,  $|\Psi_{vw}\rangle$  can be written as

$$|\Psi_{vw}\rangle = e^T \left( 1 + S_1 + \frac{1}{2} S_1^2 + S_2 + R \right) |\Phi_{vw}\rangle. \quad (14)$$

Here,  $R$  and  $|\Phi_{vw}\rangle = a_w^\dagger a_v^\dagger |\Phi_0\rangle$ , are the CC operator and the Dirac-Fock reference state for the two-valence sector, respectively. For a two-valence atom with  $N$ -electrons, the operator  $R$  is

$$R = \sum_{i=1}^N R_i, \quad (15)$$

and in CCSD approximation  $R = R_2$ . As  $R_2$  operates only on the valence electrons, it generates excited states like  $|\Phi_{vw}^{pq}\rangle$ . In the second quantized notation

$$R_2 = \sum_{pq} r_{vw}^{pq} a_p^\dagger a_q^\dagger a_w a_v, \quad (16)$$

and are obtained by solving the RCC equation [20]

$$\langle \Phi_{vw}^{pq} | \bar{H}_N + \{\bar{H}_N S'\} + \{\bar{H}_N R_2\} | \Phi_{vw} \rangle = E_{vw}^{\text{att}} \langle \Phi_{vw}^{pq} | [S' + R_2] | \Phi_{vw} \rangle. \quad (17)$$

Here, for compact notation we have use  $S' = S_1^{(1)} + \frac{1}{2}S_1^{(1)2} + S_2^{(1)}$ . In the above equation,  $E_{vw}^{\text{att}}$  is the two-electron attachment energy and it is the difference between the correlated energy of  $(n-2)$ -electron (closed-shell) sector and  $n$ -electron (two-valence) sector,  $E_{vw} - E_0$ . Like in the one-valence case, it can be expressed as

$$E_{vw}^{\text{att}} = \epsilon_v + \epsilon_w + \Delta E_{vw}^{\text{att}}, \quad (18)$$

where  $\epsilon_v$  and  $\epsilon_w$  are the Dirac-Fock energy of the valence electrons in  $|\phi_v\rangle$  and  $|\phi_w\rangle$ , respectively. And,  $\Delta E_{vw}^{\text{att}} = \Delta E_{vw}^{\text{corr}} - \Delta E_0^{\text{corr}}$ , is the difference of the correlation energies of closed-shell and two-valence sectors.

### III. TWO-VALENCE PROPERTIES CALCULATION

#### A. Hyperfine matrix elements

To illustrate the properties calculation of two-valence atomic systems using RCC we consider the example of hyperfine matrix elements. The details provided, however, are applicable to the calculation of properties associated with other one-body operators with appropriate selection rules. The hyperfine interaction is a measure of the strength of the coupling between the nuclear electromagnetic moments and the electromagnetic fields of atomic electrons. The hyperfine interaction Hamiltonian is [24]

$$H_{\text{hfs}} = \sum_i \sum_{k,q} (-1)^q t_q^k(\hat{\mathbf{r}}_i) T_{-q}^k, \quad (19)$$

where  $t_q^k(\mathbf{r})$  and  $T_q^k$  are the irreducible tensor operators of rank  $k$  in the electronic and nuclear sectors, respectively. Based on parity selection rules, the multipoles  $k = 1$  and  $k = 2$  correspond to magnetic dipole and electric quadrupole, respectively.

Using the RCC wave function from Eq. (14) we can write the expression for hyperfine matrix element in the electronic sector as

$$\langle \Psi_i | H_{\text{hfs}}^e | \Psi_j \rangle = \sum_{kl} c_k^i c_l^j \left[ \langle \Phi_k | \tilde{H}_{\text{hfs}}^e + \tilde{H}_{\text{hfs}}^e (S' + R_2) + (S' + R_2)^\dagger \tilde{H}_{\text{hfs}}^e + (S' + R_2)^\dagger \tilde{H}_{\text{hfs}}^e (S' + R_2) | \Phi_l \rangle \right], \quad (20)$$

where,  $H_{\text{hfs}}^e$  is the electronic component of the hyperfine operator in Eq. (19). And, for compact notation, we represent the two-valence state  $|\Phi_{vw}\rangle$  with  $|\Psi_i\rangle$ . And,  $c_j^i$  represents the mixing coefficient in the expansion of a multireference configuration state function  $|\Phi_i\rangle$ , and obtained by diagonalizing the  $H^{\text{DCB}}$  matrix within the chosen model space. The dressed hyperfine Hamiltonian  $\tilde{H}_{\text{hfs}}^e = e^{T^\dagger} H_{\text{hfs}}^e e^T$ , is a non terminating series of closed-shell CC operator  $T$ . In our previous work, Ref. [25], we proposed a scheme to include a class of dominant diagrams to all order in  $T$  iteratively in the dressed Hamiltonian, and based on our findings we concluded that the terms higher than quadratic in  $T$  contribute less than 0.1% to the properties. So, in the present work we truncate  $\tilde{H}_{\text{hfs}}^e$  after the second-order in  $T$  and include the terms  $\tilde{H}_{\text{hfs}}^e \approx H_{\text{hfs}}^e + H_{\text{hfs}}^e T + T^\dagger H_{\text{hfs}}^e + T^\dagger H_{\text{hfs}}^e T$  in the calculation of the properties.

Next we consider the expression of the hyperfine matrix element in Eq. (20) and separate it into sector wise contributions

$$\langle \Psi_i | H_{\text{hfs}}^e | \Psi_j \rangle = \langle \Psi_i | H_{\text{hfs}}^e | \Psi_j \rangle_{\text{DF}} + \langle \Psi_i | H_{\text{hfs}}^e | \Psi_j \rangle_{1v} + \langle \Psi_i | H_{\text{hfs}}^e | \Psi_j \rangle_{2v}. \quad (21)$$

Here, the first, second, and third terms denote the contributions from the Dirac-Fock, one-valence, and two-valence sectors, respectively. Below we discuss the contributing terms and some dominant diagrams in each of these three categories.

#### 1. Dirac-Fock contribution

Among the three terms in Eq. (21), the Dirac-Fock is expected to have the dominant contribution. It is the expectation of the bare hyperfine Hamiltonian operator with respect to the atomic state

$$\langle \Psi_i | H_{\text{hfs}}^e | \Psi_j \rangle_{\text{DF}} = \sum_{kl} c_k^i c_l^j \langle \Phi_k | H_{\text{hfs}}^e | \Phi_l \rangle. \quad (22)$$

In terms of Goldstone diagrams, there is only one diagram, Fig. 2(a), which contributes to this. Since  $H_{\text{hfs}}^e$  is an one-body operator, the contribution is the expectation of  $H_{\text{hfs}}^e$  with respect to a valence orbital and then coupling with a spectator valence orbital. The associated angular momentum diagram is topologically equivalent to the one in Fig. 1 with the effective operator  $H_{\text{hfs}}^{\text{eff},k}$  replaced by a bare hyperfine operator  $H_{\text{hfs}}^k$ . The labels  $j_v, j_w, \dots, (J_i, J_j)$  denote the angular momentum quantum numbers of uncoupled (coupled) states, and multipole  $k$  represents the rank of the hyperfine operator.

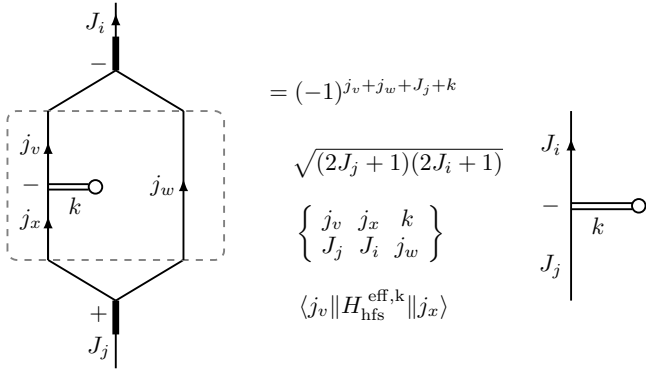


FIG. 1. Angular factor arising from the coupling of one-body effective operator and a spectator valence line. The free diagram on the right-hand side represents the geometrical part in the Wigner-Eckart theorem.

## 2. $\langle \Psi_i | H_{\text{hfs}}^e | \Psi_i \rangle_{1v}$ contribution

The next contribution is attributed to the combined effect from the closed-shell and one-valence CC operators. From Eq. (20) we can separate this contribution as

$$\begin{aligned} \langle \Psi_i | H_{\text{hfs}}^e | \Psi_j \rangle_{1v} = & \sum_{kl} c_k^* c_l^j \left[ \langle \Phi_k | \left( H_{\text{hfs}}^e T_1 + T_1^\dagger H_{\text{hfs}}^e T_2 \right. \right. \\ & + \tilde{H}_{\text{hfs}}^e S_1 + \tilde{H}_{\text{hfs}}^e S_2 + S_1^\dagger \tilde{H}_{\text{hfs}}^e S_2 \Big) + \text{h.c.} \\ & \left. \left. + T_1^\dagger H_{\text{hfs}}^e T_1 + T_2^\dagger H_{\text{hfs}}^e T_2 S_1^\dagger \tilde{H}_{\text{hfs}}^e S_1 + S_2^\dagger \tilde{H}_{\text{hfs}}^e S_2 | \Phi_l \rangle \right] \right] \quad (23) \end{aligned}$$

The diagrams corresponding to the above terms have a pair of free valence lines. As example, in Fig. (2), we give one diagram from each of the terms in Eq. (23). For easy identification the diagrams follow the same sequence as the terms. The dominant contributions are expected from  $\tilde{H}_{\text{hfs}}^e S$  and  $S^\dagger \tilde{H}_{\text{hfs}}^e$ , example diagrams from  $\tilde{H}_{\text{hfs}}^e S$  are Fig. (2) (d) and (e). The next leading order contribution are expected to be the terms with two orders of one-valence CC operators,  $S^\dagger \tilde{H}_{\text{hfs}}^e S$ . The example diagrams corresponding to this term are Fig. (2)(f), (i) and (j). To compute the contribution from  $\langle \Psi_i | H_{\text{hfs}}^e | \Psi_j \rangle_{1v}$ , first we compute the matrix elements with respect to uncoupled states and store them in the form of an one-body effective operator, and then, like in the DF, this effective operator is coupled with a spectator valence state. The angular factor arising as a result of this coupling is shown in Fig. 1.

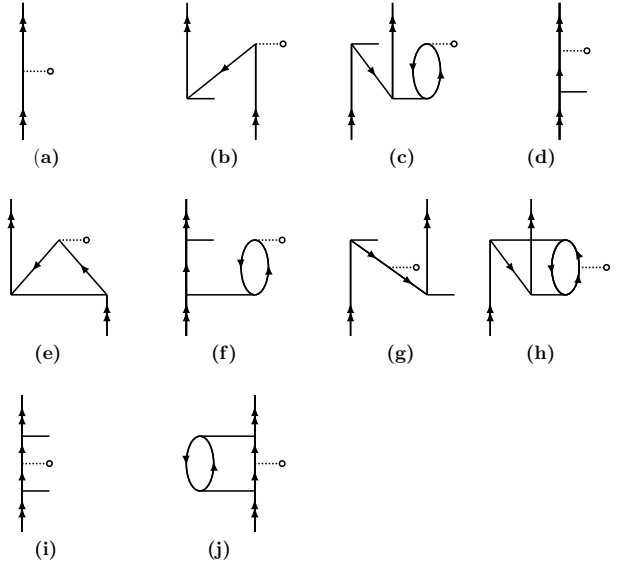


FIG. 2. (a) The DF diagram. (b-j) Some example diagrams contributing to Eq. (23) and are given in the same sequence as the terms in Eq. (23)

## 3. $\langle \Psi_i | H_{\text{hfs}}^e | \Psi_i \rangle_{2v}$ contribution

This term has contributions from all types of CC operators (the closed-shell, one-valence, and two-valence).

$$\begin{aligned} \langle \Psi_i | H_{\text{hfs}}^e | \Psi_j \rangle_{2v} = & \sum_{kl} c_k^i c_l^j \left[ \langle \Phi_k | \left( T_1^\dagger H_{\text{hfs}}^e T_2 + \tilde{H}_{\text{hfs}}^e S_2 \right. \right. \\ & + \tilde{H}_{\text{hfs}}^e R_2 + S_1^\dagger \tilde{H}_{\text{hfs}}^e S_2 + (S_1 + S_2)^\dagger \tilde{H}_{\text{hfs}}^e R_2 \\ & \left. \left. + S_1^2 \tilde{H}_{\text{hfs}}^e (S_2 + R_2) \right) + \text{h.c.} + T_2^\dagger H_{\text{hfs}}^e T_2 + S_2^\dagger \tilde{H}_{\text{hfs}}^e S_2 \right. \\ & \left. + R_2^\dagger \tilde{H}_{\text{hfs}}^e R_2 | \Phi_l \rangle \right] \quad (24) \end{aligned}$$

Like in the case of one-valence, in this case as well we give one diagram from each of the terms in the above equation in Fig. 3. Among all the terms, we expect dominant contributions from the terms  $\tilde{H}_{\text{hfs}}^e R_2$  and  $R_2^\dagger \tilde{H}_{\text{hfs}}^e$  and example diagrams are Fig. 3 (c) and its h.c. diagram. This is on account of two important reasons. First, these are the lowest order terms in  $R_2$ . And second, the magnitude of  $R_2$  is much larger than the one-valence and closed-shell CC operators,  $S$  and  $T$ , respectively. The next dominant contribution is expected from the terms  $\tilde{H}_{\text{hfs}}^e S_2$  and  $S_2^\dagger \tilde{H}_{\text{hfs}}^e$ , and example diagrams are Fig. 3 (b) and corresponding h.c. diagram, as these are one order in one-valence CC operator. Among the terms with two or higher orders CC operators, the dominant contribution is anticipated from the term  $R_2^\dagger \tilde{H}_{\text{hfs}}^e R_2$  (diagram (k)). The reason for this, as mentioned earlier, is attributed to the large magnitudes of  $R_2$  operators. The remaining terms are expected to have smaller contributions. Like the DF and one-valence contributions, all terms in Eq. (24) are computed with respect to uncoupled states first and then store in the form of a two-body effective operator, shown by the dashed rectangle in Fig. 4,

and then coupled using the angular momentum algebra to obtain the contribution at the level of two-valence. The angular factor arising from this coupling is given in the Fig. 4.

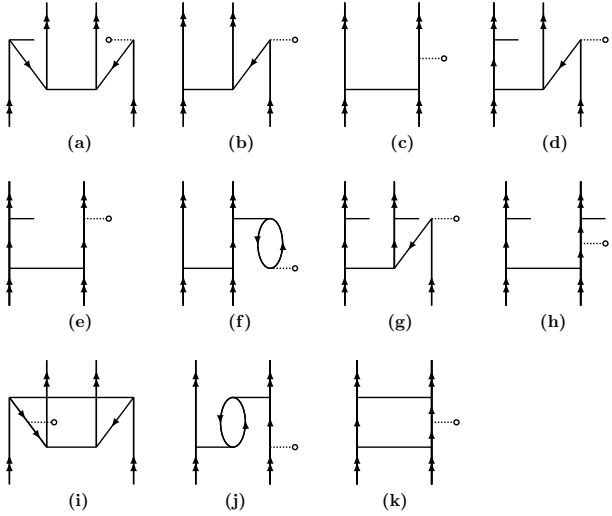


FIG. 3. Some example diagrams contributing to Eq. (24). For easy identification, diagrams are given in the same sequence as the terms in Eq. (24)

### B. Perturbative $R_3$

To account for the electron correlation effects from triple excitations, we resort to the perturbative triples. With this approach we can incorporate the dominant contributions from triple excitations, however, with far less computational cost than the full triples. For this, we choose the triples which arise from the two-valence CC operator  $R_2$ , viz. from the term  $\bar{g}R_2$ , where  $g_{ij} = \sum_{i < j} (\frac{1}{r_{ij}} + g^B(r_{ij}))$ , a two-body residual interaction. This is the dominant contribution to triples, since the magnitude of  $R_2$  is larger than  $T$  and  $S$  for two-valence systems. There is one diagram from the term  $\bar{g}R_2$ , shown in

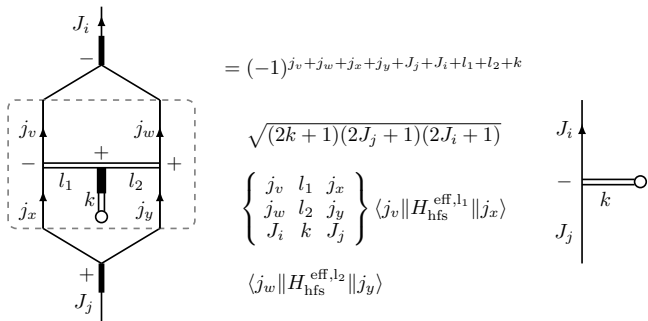


FIG. 4. Angular factor arising from the coupling of two-body effective operator. Portion in the dashed rectangle is an effective operator which subsumes contribution from Eq. (24) in terms of uncoupled states.

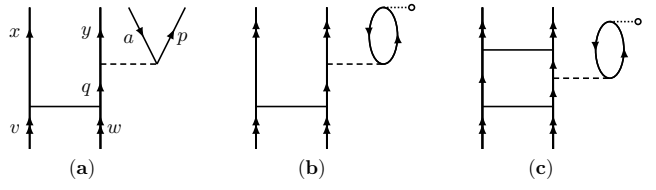


FIG. 5. Diagrams representing the perturbative  $R_3$  (diagram (a)), and the hyperfine matrix element arising from the terms  $H_{\text{hfs}}^e R_3$  and  $R_2^\dagger H_{\text{hfs}}^e R_3$  (diagrams (b) and (c), respectively). The dashed line represents the two-body residual interaction between the electrons.

Fig. 5 (a), and based on this the algebraic expression for perturbative  $R_3$  is

$$R_3 \approx \frac{1}{\Delta \epsilon_{vwa}^{xyp}} a_x^\dagger a_y^\dagger a_p^\dagger a_a a_w a_v \sum_q \langle y p | g | q a \rangle \langle x q | R_2 | v w \rangle, \quad (25)$$

where  $\Delta \epsilon_{vwa}^{xyp} = \epsilon_v + \epsilon_w + \epsilon_a - \epsilon_x - \epsilon_y - \epsilon_p$ . The operator  $R_3$  can now contract with other CC operators along with the hyperfine operator and contribute to the properties at two-valence through Eq. (20). Based on our analysis at the CCSD level, however, we find that the most dominant contributions to the properties are from the terms with  $R_2$  operators only, viz.  $H_{\text{hfs}}^e R_2$ ,  $R_2^\dagger H_{\text{hfs}}^e$  and  $R_2^\dagger H_{\text{hfs}}^e R_2$ . And, the terms with operators  $T$  and  $S$  have very small contributions. So, in the present work, to account the contribution from  $R_3$  we include the terms  $H_{\text{hfs}}^e R_3$ ,  $R_3^\dagger H_{\text{hfs}}^e$ ,  $R_2^\dagger H_{\text{hfs}}^e R_3$  and  $R_3^\dagger H_{\text{hfs}}^e R_2$ . There are 3 diagrams each from these terms which will contribute to the properties at two-valence. And, as an example, we give one diagram each from the terms  $H_{\text{hfs}}^e R_3$  and  $R_2^\dagger H_{\text{hfs}}^e R_3$  in Fig. 5 (b) and Fig. 5 (c), respectively.

### C. Hyperfine induced E1 transition

The hyperfine interactions in atoms couple the electronic angular momentum  $J$  with the nuclear spin  $I$  to give a total angular momentum  $F$ . As a result, we can represent a hyperfine eigenstate as  $|\Gamma F M_F\rangle$ , where  $M_F$  represents the magnetic quantum number, and both  $F$  and  $M_F$  are good quantum numbers. Considering the hyperfine interaction  $H_{\text{hfs}}$  as a perturbation, using the first-order perturbation theory we can write

$$|\Gamma F M_F\rangle = \sum_n \left[ \frac{\langle (\gamma_n J_n \gamma_I I) F M_F | H_{\text{hfs}} | (\gamma_0 J_0 \gamma_I I) F M_F \rangle}{E_{J_0} - E_{J_n}} \right] \times |\langle (\gamma_n J_n \gamma_I I) F M_F \rangle, \quad (26)$$

where the term with the square parenthesis represents the mixing of unperturbed  $|\gamma_0 (J_0 I) F M_F\rangle$  state with an excited  $|\gamma_n (J_n I) F M_F\rangle$  state through the hyperfine interaction. The parameters  $\Gamma$ ,  $\gamma_n$  and  $\gamma_0$  are the additional quantum numbers, used to specify the states uniquely. The energy  $E_J$  in the denominator is the exact energy obtained from the solution of the Eq. (13).

The electric dipole transition probability between two hyperfine levels  $|\Gamma_i F_i M_{F_i}\rangle$  and  $|\Gamma_j F_j M_{F_j}\rangle$  is defined as

$$A = \frac{2.02612 \times 10^{18}}{\lambda^3 (2F_i + 1)} |\langle \Gamma_i F_i || \mathbf{D} || \Gamma_j F_j \rangle|^2, \quad (27)$$

where  $\lambda$  is the wavelength in angstrom and  $\mathbf{D}$  is the electric dipole operator. Using the expression of hyperfine wave function from Eq. (26), the transition probability is

---


$$A = \frac{2.02612 \times 10^{18}}{\lambda^3 (2F_i + 1)} \times \left| \sum_n \frac{\langle (\gamma_i J_i \gamma_{II}) F_i M_{F_i} || \mathbf{D} || (\gamma_n J_n \gamma_{II}) F_n M_{F_n} \rangle \langle (\gamma_n J_n \gamma_{II}) F_n M_{F_n} | H_{\text{hfs}} | (\gamma_j J_j \gamma_{II}) F_j M_{F_j} \rangle}{E_{J_j} - E_{J_n}} \right|^2 \quad (28)$$

Here, the dipole and hyperfine matrix elements are [24, 26]

$$\langle (\gamma_i J_i \gamma_{II}) F_i M_{F_i} || \mathbf{D} || (\gamma_n J_n \gamma_{II}) F_n M_{F_n} \rangle = \sqrt{(2F_n + 1)(2F_i + 1)} (-1)^{J_i + I + F_n + 1} \begin{Bmatrix} F_i & 1 & F_n \\ J_n & I & J_i \end{Bmatrix} \langle \gamma_i J_i || D || \gamma_n J_n \rangle \quad (29)$$

and

$$\begin{aligned} \langle (\gamma_n J_n, \gamma_{II}) F_n M_{F_n} | H_{\text{hfs}} | (\gamma_j J_j, \gamma_{II}), F_j M_{F_j} \rangle &= \delta(F_n, F_j) \delta(M_{F_n}, M_{F_j}) \mu_I \left[ \frac{(I+1)(2I+1)}{I} \right] (-1)^{J_j + I + F_n} \begin{Bmatrix} J_n & J_j & 1 \\ I & I & F_n \end{Bmatrix} \\ &\times \langle \gamma_n J_n || t^1 || \gamma_j J_j \rangle, \end{aligned} \quad (30)$$


---

respectively. In deriving equation (30) we have used

$$\langle \gamma_I I || T^1 || \gamma_I I \rangle = \mu_I \sqrt{\frac{(I+1)(2I+1)}{I}},$$

where,  $\mu_I$  is the nuclear magnetic dipole moment. The reduced matrix elements  $\langle \gamma_i J_i || D || \gamma_n J_n \rangle$  and  $\langle \gamma_n J_n || t^1 || \gamma_j J_j \rangle$  are calculated using the wave functions obtained from FSRCC discussed in the previous subsection.

#### IV. CALCULATIONAL DETAILS

##### A. Basis set

To obtain the accurate results for properties using RCC it is critical to use a basis set which provides a good description of single-electron wave functions and energies. In this work we use the Gaussian-type orbitals (GTOs) [21] as the single-electron basis for RCC calculations. The GTOs are the finite basis sets in which the single-electron wave functions are expressed as a linear combination of the Gaussian-type functions (GTFs). More precisely, the GTFs of the large component of the single-electron wave function is expressed as

$$g_{\kappa p}^L(r) = C_{\kappa p}^L r^{n_\kappa} e^{-\alpha_p r^2}, \quad (31)$$

where  $p = 0, 1, 2, \dots, N$  is the GTO index and  $N$  is the total number of GTFs. The exponent  $\alpha_p$  is further expressed as  $\alpha_0 \beta^{p-1}$ , where  $\alpha_0$  and  $\beta$  are the two independent parameters. The parameters  $\alpha_0$  and  $\beta$  are optimized separately for each orbital symmetry so that the single-electron wave functions and energies match well with the numerical orbitals obtained

from the GRASP2K [27]. The small components of single-electron wave function are derived from the large components using the kinetic balance condition [22]. And, to incorporate the effects of finite charge distribution of the nucleus we use a two-parameter finite size Fermi density distribution

$$\rho_{\text{nuc}}(r) = \frac{\rho_0}{1 + e^{(r-c)/a}}, \quad (32)$$

where,  $a = t4 \ln(3)$ . The parameter  $c$  is the half charge radius of the nucleus so that  $\rho_{\text{nuc}}(c) = \rho_0/2$ , and  $t$  is the skin thickness. In our recent work, Ref. [17], we have given the optimized values of  $\alpha_0$  and  $\beta$ , and have also compared the single-electron as well as the self-consistent field energies for group-13 ions. The single-electron basis used in the properties calculations in the present work also incorporates the effects of Breit interaction, vacuum polarization and the self-energy corrections.

#### V. RESULTS AND DISCUSSIONS

##### A. Basis convergence

Since the GTO basis are not mathematically complete, convergence of properties results with basis size is critical to obtain the reliable results in FSRCC calculations. To show the convergence trend, in Table I we list the values of excitation energies, hyperfine structure constants and E1 transition amplitudes for different basis sizes. For this, as using the DCB Hamiltonian is more compute intensive, we use the Dirac-Coulomb (DC) Hamiltonian. And, this is a suitable choice as the correlation effects associated with the Breit interaction is

much smaller compared to the Coulomb interaction. As discernible from the table, to obtain a converged basis we start with a moderate basis size of 86 orbitals and add orbitals in each symmetry systematically until the change in the properties is less than or equal to  $10^{-3}$  in respective units of the above properties. From the table, for example, the change in the hyperfine structure constants is less than  $10^{-3}$  MHz when the basis is augmented from 167 to 173. So, to minimize the compute time, we consider the basis set with 167 orbitals as optimal, and use it for further FSRCC calculations where, to further improve the accuracy of the properties results, the corrections from the Breit interaction, vacuum polarization and the self-energy are incorporated.

## B. Excitation energies

The eigenvalues obtained from the solution of the eigenvalue equation (13) are used to calculate the excitation energies of various excited states. The excitation energy of a state  $nl n' l' (2S+1) L_J$  is defined as

$$\Delta E_{nl n' l' (2S+1) L_J} = E_{nl n' l' (2S+1) L_J} - E_{ns^2 1S_0}, \quad (33)$$

where  $E_{ns^2 1S_0}$  and  $E_{nl n' l' (2S+1) L_J}$  are the exact energies of the ground and excited states, respectively. In Table II, we list the energies from our calculations along with other theory and experimental data for comparison. In a separate column we also provide the cumulative contributions from Breit and QED corrections. As evident from the table, energies are calculated in three steps. We start with the configuration  $3s^2 + 3s3p$  in the model space and then include  $3s4s$  and  $3p^2 + 3s3d$  in two subsequent calculations CF2 and CF3, respectively. We could not separate the contribution of  $3p^2$  from  $3s3d$  because inclusion of any one of these alone leads to divergence of FSRCC calculations due to *intruder* states: When the configuration  $3p^2$  is included,  $3s3d 3D_{1,2,3}$  states lies well within the energy range of the model states, and hence lead to divergence due to small energy denominator. Similarly, when  $3s3d$  is included,  $3p^2 3P_{0,1,2}$  states lead to a divergence.

As we observe from the entries in the table (and also see in the Fig. 6), though only the states from the configurations  $3s^2$  and  $3s3p$  are relevant for clock transition properties, inclusion of  $3p^2$ ,  $3s3d$  and  $3s4s$  in the model space leads to two important improvements. First, it improves the energies of  $3s^2 1S_0$  and  $3P_{0,1,2}$  states. Quantitatively, the relative error reduces to  $\approx 0.45\%$ ,  $0.004\%$ ,  $0.01\%$  and  $0.07\%$  from  $0.53\%$ ,  $0.35\%$ ,  $0.50\%$  and  $0.81\%$ , respectively. This could be attributed to the more *valence-to-valence* correlation effects incorporated through the effective Hamiltonian. For  $1P_1^o$  state, we however observe an opposite trend of deteriorating excitation energy. But this will have a negligible effect on the value of the life time of  $3P_0^o$  as the energy separation  $\Delta E_{1P_1^o}$  is very high,  $\approx 22457 \text{ cm}^{-1}$ . Second, and more importantly, it also improves the energy separation  $\Delta E_{3P_1^o} = E_{3P_0^o} - E_{3P_1^o}$ , which is critical to obtain the accurate value of the life time of  $3P_0^o$ . Quantitatively,  $\Delta E_{3P_1^o}$  increases to  $57.76 \text{ cm}^{-1}$ , very close to the experimental separation  $60.88 \text{ cm}^{-1}$ , from  $8.24 \text{ cm}^{-1}$ . In

terms of percentage, there is a reduction in the error from  $\approx 86\%$  to  $5\%$ .

Comparing our energy results with experiment and previous calculations, our results are in good agreement with experiment as well as previous theory results for all the states. The smallest and largest relative errors in our calculations are  $0.004\%$  and  $0.9\%$ , respectively. These are observed in the case of  $3P_0^o$  and  $3p^2 3P_2$  states, respectively. For the other states, errors lie in-between, with the states from configurations  $3s^2$  and  $3s3p$  more accurate than those from the high energy configurations. Among the previous theory results, the most accurate results are from the CI+AO calculations by Konovalova and collaborators [29] and Safranova and collaborators [11]. The maximum relative error is about  $0.14\%$  in each calculations in the case of  $3s3d 3D_2$  and  $1P_1^o$  states, respectively. The next accurate results are from the CICP calculation by Mitroy and collaborators [30]. The maximum error is about  $0.05\%$ , in the case of  $3P_0^o$  state. The remaining results are either based on many-body perturbation theory or multi-configuration Hartree-Fock and its variations, and are not very accurate. Considering the contributions from the Breit and QED corrections, we observe the largest cumulative contribution of about  $0.01\%$  of the total value in the case of  $3P_0^o$ . This small contribution is in agreement with the previous calculation [29], however, with opposite phase.

## C. Hyperfine reduced matrix elements and structure constants

We present the magnetic dipole and electric quadrupole hyperfine constants ( $A$  and  $B$ , respectively) for  $3P_1^o$ ,  $3P_2^o$  and  $1P_1^o$  in Table III. And, the magnetic dipole hyperfine off-diagonal reduced matrix elements  $\langle 3P_1^o || t^1 || 3P_0^o \rangle$  and  $\langle 1P_1^o || t^1 || 3P_0^o \rangle$ , which contribute to the E1HFS amplitude are given in the Table IV. To assess the actual contributions from Breit, QED and dominant triples, these are presented in separate rows in both the tables. As discernible from the Table III, and as to be expected, the dominant contribution is from the CCSD for all the states. And, among the terms within the CCSD, as listed in the Table V, the Dirac-Fock (DF) has the largest contribution in all the cases. Quantitatively, it contributes  $\approx 93.2$ ,  $93.6$ ,  $103$ ,  $91.6$ ,  $115$  and  $106\%$  of the total value for  $A(3P_1^o)$ ,  $A(3P_2^o)$ ,  $A(1P_1^o)$ ,  $B(3P_1^o)$ ,  $B(3P_2^o)$  and  $B(1P_1^o)$ , respectively. There is a mixed pattern for the next dominant contribution. The term  $1v$  has more contribution than  $2v$  for  $A(3P_1^o)$ ,  $A(3P_2^o)$  and  $B(3P_1^o)$ . However, the pattern is opposite for  $A(1P_1^o)$ ,  $B(3P_2^o)$  and  $B(1P_1^o)$ . The other important point to notice is that the contribution from  $2v$  is opposite to  $1v$  and DF values in all the cases, which reduces the total value due to cancellation. Among the terms within  $2v$ , we find that the largest contribution is from the term  $H_{\text{hfs}}^e R_2 + \text{h.c.}$  This is attributed to the larger magnitude of the  $R_2$  operator.

Considering the contribution from perturbative triples, it has the largest contributions of  $\approx 3$  and  $5\%$  of the total value for  $A$  and  $B$ , respectively. For  $A$  it is in the case of  $1P_1^o$ , however, for  $B$  it is in the  $3P_2^o$  state. Such large contributions indicate that the triples must be included in the FSRCC calcu-

TABLE I. Convergence of excitation energy, hyperfine structure constants and electric dipole transition amplitudes as function of basis size.

States/Property	Basis size							
	BS1	BS2	BS3	BS4	BS5	BS6	BS7	BS8
				Exc. ene.				
$3s3p\ ^3P_0^o$	36880.92	36887.02	36893.38	37050.55	37388.70	37391.43	37391.43	37391.43
$3s3p\ ^3P_1^o$	36941.51	36947.51	36953.75	37109.51	37448.96	37449.19	37449.19	37449.19
$3s3p\ ^3P_2^o$	37050.77	37056.56	37062.55	37215.38	37557.29	37552.51	37552.52	37552.52
$3s3p\ ^1P_1^o$	60174.87	60177.54	60181.35	60186.27	60205.24	60109.38	60109.38	60109.38
$3p^2\ ^1D_2$	84935.91	84943.85	84951.80	85142.41	85605.12	85574.35	85574.35	85574.35
$3s4s\ ^3S_1$	90488.94	90494.85	90500.30	90670.08	91019.53	91041.40	91041.40	91041.40
$3p^2\ ^3P_0$	92789.16	92801.94	92816.68	92977.64	93367.32	93374.60	93374.59	93374.59
$3p^2\ ^3P_1$	92798.39	92810.12	92823.73	92986.81	93380.10	93375.69	93375.69	93375.69
$3p^2\ ^3P_2$	92882.82	92894.07	92907.51	93053.81	93411.63	93405.18	93405.18	93405.18
$3s4s\ ^1S_0$	94524.80	94531.58	94537.68	94717.64	95132.51	95154.58	95154.59	95154.58
$3s3d\ ^3D_1$	94950.56	94948.62	94943.20	95034.90	95321.19	95246.39	95246.39	95246.39
$3s3d\ ^3D_2$	94954.45	94952.51	94947.56	95039.24	95325.07	95250.27	95250.27	95250.27
$3s3d\ ^3D_3$	94957.27	94955.31	94950.02	95041.37	95326.47	95251.68	95251.68	95251.68
$3s3d\ ^1D_2$	109929.38	109931.55	109931.47	110085.40	110457.19	110379.43	110379.43	110379.43
$3p^2\ ^1S_0$	111441.00	111448.22	111453.87	111532.23	111733.69	111593.71	111593.71	111593.71
				HFS con.				
$A(^3P_1^o)$	1345.337	1357.349	1370.930	1376.918	1385.889	1385.409	1385.410	1385.410
$A(^3P_2^o)$	1147.931	1159.867	1173.480	1178.863	1187.596	1188.024	1188.025	1188.025
$A(^1P_1^o)$	283.646	283.920	284.187	286.985	291.088	292.588	292.588	292.588
$B(^3P_1^o)$	-15.969	-15.978	-15.980	-16.059	-16.165	-16.173	-16.173	-16.173
$B(^3P_2^o)$	25.026	25.041	25.045	25.231	25.503	25.549	25.549	25.549
$B(^1P_1^o)$	27.340	27.355	27.358	27.576	27.825	27.876	27.876	27.876
				E1 amp.				
$^1S_0 - ^3P_1^o$	-1.843[-2]	-1.832[-2]	-1.820[-2]	-1.718[-2]	-1.531[-2]	-1.425[-2]	-1.425[-2]	-1.425[-2]
$^1S_0 - ^1P_1^o$	2.894	2.893	2.893	2.875	2.845	2.841	2.841	2.841

<sup>a</sup> BS1 - 86 (14s, 14p, 9d, 5f, 4g, 4h)<sup>b</sup> BS2 - 97 (15s, 15p, 10d, 6f, 5g, 5h)<sup>c</sup> BS3 - 119 (17s, 17p, 12d, 8f, 7g, 7h)<sup>d</sup> BS4 - 141 (19s, 19p, 14d, 10f, 9g, 9h)<sup>e</sup> BS5 - 152 (20s, 20p, 15d, 11f, 10g, 10h)<sup>f</sup> BS6 - 161 (21s, 21p, 15d, 12f, 11g, 11h)<sup>g</sup> BS7 - 167 (23s, 23p, 15d, 12f, 11g, 11h)<sup>h</sup> BS8 - 173 (25s, 25p, 15d, 12f, 11g, 11h)

lations to obtained the accurate results for hyperfine structure and related properties for  $\text{Al}^{1+}$ . Looking into the Breit contribution, the largest contribution is  $\approx 0.9\%$ , for  $A$  in the case of  $^3P_2^o$  state. Considering the level of the accuracy needed for clock properties, it is a significant contribution and can not be neglected. The largest, and negligible, cumulative contribution of  $\approx 0.02\%$  is observed from the vacuum polarization and the self-energy corrections.

To the best our knowledge, there are no data from experiments for comparison. From other theory calculations, there is one data each for  $A$  and  $B$  for  $^3P_1^o$  and  $^3P_2^o$  using the multi-configuration-Dirac-Hartree-Fock calculation from Itano and collaborators [38]. The magnitude of our results 1389.81, 1174.29 and 16.65 for  $A(^3P_1^o)$ ,  $A(^3P_2^o)$  and  $B(^3P_1^o)$  are larger by  $\approx 3.1$ , 2.2 and 5.6%, respectively than the values reported in Ref. [38]. The reason for this difference could be attributed to the more accurate treatment of electron correlations in the present calculation, as the FSRCC accounts for the residual Coulomb interaction to all orders. We observe an op-

posite trend in the case of  $B(^3P_2^o)$ , our value 24.23 is smaller, by 45.7%, than the value 31.42 in Ref. [38]. The reason is attributed to the large cancellation due to contribution from the term  $2v$ , equation 24. Our Dirac-Fock value 29.44, given in Table V, is close to the MCDHF value 31.42 in Ref. [38]. At level of off-diagonal matrix elements, there are two results, one each from the MCDHF [13] and CI+MBPT [39] calculations, which can be used for comparison. Ref. [13] reports the values of matrix elements  $\langle(^3P_1^o I)FM_F|H_{\text{hfs}}|(^1P_1^o I)FM_F\rangle$  and  $\langle(^1P_1^o I)FM_F|H_{\text{hfs}}|(^1P_0^o I)FM_F\rangle$  as  $4.741 \times 10^{-7}$  and  $5.935 \times 10^{-7}$  atomic units, respectively. Our values  $3.838 \times 10^{-7}$  and  $4.634 \times 10^{-7}$ , respectively agree well with them. The magnitude of the reduced matrix element  $\langle^3P_0^o ||t^1||^3P_0^o\rangle$ , 0.0938 a.u., from our calculation is smaller than the CI+MBPT value, 0.1195, from Ref. [39]. The reason for this small difference is attributed to the difference in the methods employed in the two calculations.

TABLE II. Energy for ground state  $3s^2 \ ^1S_0$  and excitation energies for excited states computed using three configurations CF1, CF2, and CF3 in the model space. The values listed are using the converged basis set of 173 orbitals and in  $\text{cm}^{-1}$ .

States	CCSD			Breit + QED	Total	Other cal.	Exp. [28]
	CF1: $3s^2 + 3s3p$	CF2: $CF1+3s4s$	CF3: $CF2+3p^2 + 3s3d$				
$3s^2 \ ^1S_0$	379293.993	379408.787	379578.436	3.553	379581.988	$381210^j, 381331^d, 381287^k$ $382024^c$	381308.00
$3s3p \ ^3P_0^o$	37259.930	37323.209	37391.428	3.227	37394.655	$37392^j, 37374^k, 37396^d$ $37191^c$	37393.03
$3s3p \ ^3P_1^o$	37268.169	37346.486	37449.190	2.650	37451.839	$36705^a, 35000^b, 37454^j$ $36292^l, 37516^m, 37457^d$ $37818^n, 37253^p, 37251^c$	37453.91
$3s3p \ ^3P_2^o$	37272.795	37380.954	37552.515	2.189	37554.704	$37579^j, 37572^d, 37374^c$	37577.79
$3s3p \ ^1P_1^o$	59871.557	59966.666	60109.376	1.703	60111.079	$60723^a, 63000^b, 59855^j$ $59849^k, 59427^l, 60198^m$ $59768^d, 59140^n, 60104^p$ $54410^c$	59852.02
$3p^2 \ ^1D_2$			85574.346	3.402	85577.748	$85450^j, 85462^d, 85678^c$	85481.35
$3s4s \ ^3S_1$	90915.947		91041.401	1.194	91042.595	$91256^j, 91289^d, 91262^k$	91274.50
$3p^2 \ ^3P_0$			93374.594	4.258	93378.852	$94049^j, 94092^d, 93672^c$	94084.96
$3p^2 \ ^3P_1$			93375.687	4.357	93380.044	$94112^j, 94151^d, 93735^c$	94147.46
$3p^2 \ ^3P_2$			93405.180	3.833	93409.013	$94234^j, 94265^d, 93857^c$	94268.68
$3s4s \ ^1S_0$	95036.810		95154.584	1.335	95155.919	$95336^j, 95354^d$	95350.60
$3s3d \ ^3D_1$			95246.393	1.917	95248.310	$95420^j, 95527^d, 95532^k$ $95695^c$	95551.44
$3s3d \ ^3D_2$			95250.266	1.797	95252.063	$95419^j, 95527^d, 95697^c$	95550.51
$3s3d \ ^3D_3$			95251.677	1.730	95253.407	$95418^j, 95524^d, 95690^c$	95549.42
$3s3d \ ^1D_2$			110379.435	2.381	110381.816	$106270^c$	110089.83
$3p^2 \ ^1S_0$			111593.713	3.996	111597.709		111637.33

<sup>j</sup>Ref.[29][CI+AO], <sup>k</sup>Ref.[30][CICP], <sup>d</sup>Ref.[11][CI+AO], <sup>a</sup>Ref.[31][CIDF+CP], <sup>b</sup>Ref.[32][MCDF], <sup>l</sup>Ref.[33][MCRRPA],  
<sup>m</sup>Ref.[34][MCDHF], <sup>n</sup>Ref.[35][RMBPT] <sup>p</sup>Ref.[36][MCDF] <sup>c</sup>Ref.[37][RMBPT]

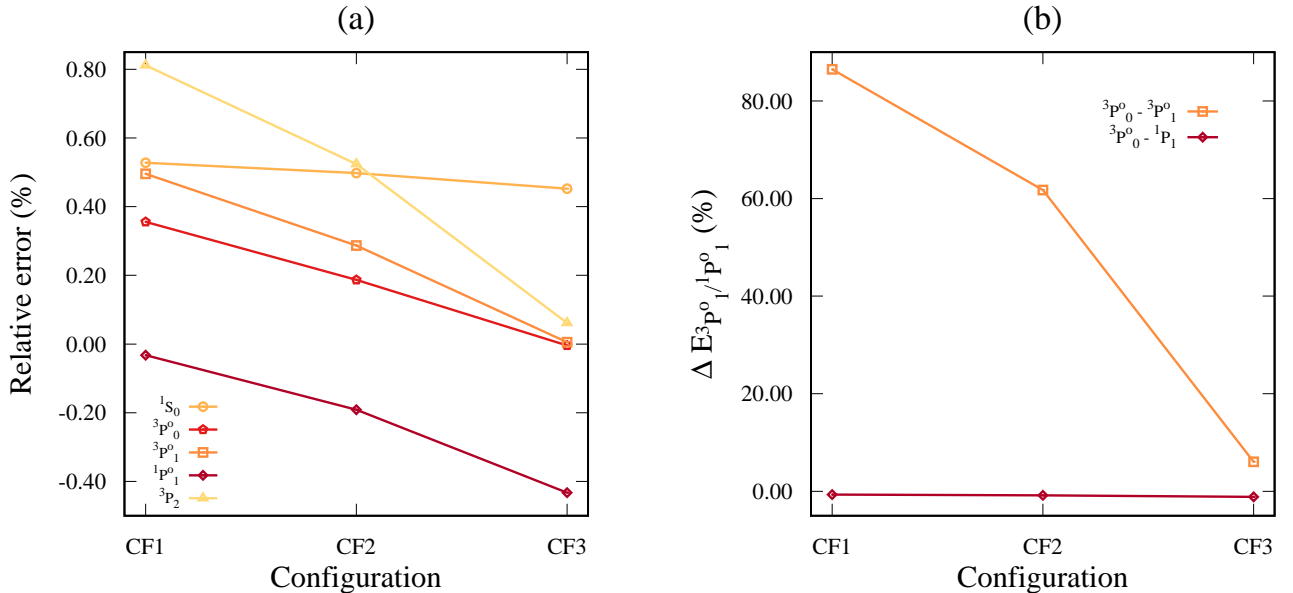


FIG. 6. The relative errors in excitation energy and energy separation as a function of configurations, figures (a) and (b), respectively.

TABLE III. Magnetic dipole and electric quadrupole hyperfine structure constants (in MHz) for states  ${}^3P_1^o$ ,  ${}^3P_2^o$  and  ${}^1P_1^o$ . The values of the nuclear magnetic dipole moment  $\mu_I = 3.6415069(7)\mu_N$  and electric quadrupole moment  $Q = 0.1466(10)b$  are used in the calculation.

Methods	Hyperfine Structure Constants					
	A			B		
	${}^3P_1^o$	${}^3P_2^o$	${}^1P_1^o$	${}^3P_1^o$	${}^3P_2^o$	${}^1P_1^o$
CCSD	1385.409	1188.024	292.588	-16.173	25.549	27.876
CCSD(T)	8.316	-3.865	-8.661	-0.473	-1.276	0.432
Breit	-4.240	-10.194	2.153	-1.633[-4]	1.246[-3]	-2.745[-4]
Vacuum pol.	0.306	0.306	-4.118[-4]	4.069[-5]	-3.715[-5]	-1.956[-4]
Self-energy	0.023	0.023	3.790[-4]	2.561[-6]	4.323[-5]	3.966[-5]
Total	1389.814	1174.294	286.0800	-16.646	24.274	28.308
Other cal.	1348 <sup>a</sup>	1149 <sup>a</sup>		-15.62 <sup>a</sup>	31.42 <sup>a</sup>	

<sup>a</sup>Ref.[38][MCDHF],

TABLE IV. Magnetic dipole hyperfine and E1 transition reduced matrix elements (in a.u.).

Methods	$\langle {}^1S_0    d    {}^3P_1^o \rangle$	$\langle {}^1S_0    d    {}^1P_1^o \rangle$	$\langle {}^3P_1^o    t^1    {}^3P_0^o \rangle$	$\langle {}^1P_1^o    t^1    {}^3P_0^o \rangle$
CCSD	-1.425[-2]	2.841	-0.0954	0.0785
CCSD(T)	-9.384[-4]	-9.159[-4]	1.608[-3]	-5.667[-4]
Breit	6.303[-5]	-2.069[-5]	4.882[-5]	-3.165[-4]
Vacuum pol.	-9.737[-7]	1.181[-5]	-4.198[-5]	3.035[-5]
Self-energy	2.332[-7]	5.608[-7]	-2.993[-6]	2.849[-6]
Total	-1.513[-2]	2.840	-0.0938	0.0776

TABLE V. Contributions from Dirac-Fock, one-valence and two-valence terms, as in Eq. (21), to the properties. The values of  $A$  and  $B$  are given in MHz, and E1 amplitudes are in a.u.

Property	DF	1v	2v	Total
$A({}^3P_1^o)$	1291.188	266.914	-172.694	1385.409
$A({}^3P_2^o)$	1112.166	225.722	-149.864	1188.024
$A({}^1P_1^o)$	300.166	66.072	-73.650	292.588
$B({}^3P_1^o)$	-14.815	-4.608	3.250	-16.173
$B({}^3P_2^o)$	29.436	8.744	-12.631	25.549
$B({}^1P_1^o)$	29.533	8.780	-10.637	27.876
$E1({}^1S_0 - {}^3P_1^o)$	1.934[-3]	7.567[-4]	-1.694[-2]	-1.425[-2]
$E1({}^1S_0 - {}^1P_1^o)$	2.346	-0.055	0.550	2.841

#### D. E1 Transition amplitudes and oscillator strengths

The E1 transition reduced matrix elements in Table IV are converted to oscillator strengths and presented in the Table VI along with other theory and experimental results for comparison. Like hyperfine structure constants and matrix elements, the dominant contribution is from the CCSD. It contributes more than 94% of the total value. The contributions from the perturbative triples and Breit interactions are not negligible. The maximum contributions from these are  $\approx 6.2$  and  $0.4\%$ , respectively. Like the case of hyperfine, vacuum polarization and self-energy have negligible contributions.

From experiments, to the best of our knowledge, *one* and *three* experimental results of oscillator strength for  ${}^1S_0 - {}^3P_1^o$

[40] and  ${}^1S_0 - {}^1P_1^o$  transitions [41–43], respectively are available in the literature, and all are from the old experiments. While [40] is using the time-resolve technique, the others [41–43] are using the beam-foil technique to study the atomic spectra. Our result,  $2.60 \times 10^{-5}$ , for  ${}^1S_0 - {}^3P_1^o$  transition has the same order of magnitude as the experiment,  $(1.068 \pm 0.074) \times 10^{-5}$ , however, larger by  $\approx 128\%$ . Looking into the other theory calculations, though all are MCDF and based calculations, there is a large variation in the reported results as the values lie in the range  $0.36 \times 10^{-5}$  to  $3.78 \times 10^{-5}$ . For  ${}^1S_0 - {}^1P_1^o$  transition, though all experiments have use the same measurement technique, there is large variation in the results. Also, the uncertainties in these measurements are very large, they are in the range  $\approx 4.8$  [42] to  $15.8\%$  [41, 43]. Considering the experimental uncertainties, our result 1.47 is in good agreement. In terms of other theory calculations, the reported results are very close to each other. The reason could be, the more or less same treatment of electron correlations in all the calculations as they are mostly based MCDF and its variations. Our result, 1.473, is about 20.7% smaller than the average value, 1.777, calculated from the previous works. The reason for this difference is attributed to the more accurate treatment of electron correlation effects in our calculations.

#### E. Hyperfine induced E1 transition

Using the electric dipole and hyperfine reduced matrix elements from Table IV and the energy differences  $\Delta E_{{}^3P_1^o / {}^1P_1^o}$  from Table II in Eq. (28), we calculate the E1HFS amplitude

TABLE VI. Oscillator strengths of allowed transitions compared with other calculations and experiments. Here,  $[x]$  represents  $10^x$ .

Transition	Ours	Other cal.	Expt.
$^1S_0 - ^3P_1^o$	2.604[−5]	3.560[−6] <sup>a</sup> , 8.875[−6] <sup>b</sup> , 3.776[−5] <sup>c</sup> , 1.017[−5] <sup>d</sup>	(1.068 ± 0.074)[−5] <sup>i</sup>
$^1S_0 - ^1P_1^o$	1.473	1.740 <sup>a</sup> , 1.765 <sup>e</sup> , 1.831 <sup>b</sup> , 1.850 <sup>f</sup> 1.746 <sup>g</sup> , 1.751 <sup>h</sup> , 1.76 <sup>c</sup> , 1.775 <sup>d</sup>	1.74 ± 0.27 <sup>j</sup> 1.26 ± 0.06 <sup>k</sup> , 1.9 ± 0.3 <sup>l</sup>

<sup>a</sup>Ref.[32][MCDF], <sup>b</sup>Ref.[33][MCRRPA], <sup>c</sup>Ref.[31][MCDF+CP], <sup>d</sup>Ref.[13][MCDHF], <sup>e</sup>Ref.[30][CICP], <sup>f</sup>Ref.[44][RRPA],

<sup>g</sup>Ref.[34][MCDHF], <sup>h</sup>Ref.[36][MCDF], <sup>i</sup>Ref.[40][Exp.], <sup>j</sup>Ref.[41][Exp.], <sup>k</sup>Ref.[42][Exp.] <sup>l</sup>Ref.[43][Exp.]

of  $^1S_0 - ^3P_0^o$  transition and the life time of  $^3P_0^o$  state. We present these results in Table VII. The available experimental value of life time of  $^3P_0^o$  is  $20.6 \pm 1.4$  s from Rosenband and collaborators [5]. As we observe, the error associated with this measurement is however large,  $\approx 6.8\%$ . Our calculated CCSD(T)+Breit+QED value, 20.20, is in excellent agreement with the experimental value, with a small difference of about 2%. From our calculations we find that the inclusion of the dominant triples, Breit interaction and QED corrections are important to obtain the accurate results on the E1HFS properties. Quantitatively, the contribution from the perturbative triples to the life time of  $^3P_0^o$  state is  $\approx -6.4\%$  of the total value, and it improves the value towards the experiment. And, the cumulative contribution from Breit and QED corrections is  $\approx 0.8\%$  of the total value. Considering the accuracies of atomic clocks, this is a significant contribution and can not be neglected.

Looking into other theory results, there are two results, perhaps from the same group, using the MCDF calculations [12, 13]. Between them, the revised calculation [13] treats electron correlation more accurately than the Ref. [12]. More precisely, there are two main improvements in Ref. [13]. First, both *single* and *double* replacements of electrons are considered while generating the CSFs for multiconfiguration space. However, in calculation [12], the CSFs from only *single* electron replacements are included. Second, the active space includes orbitals up to  $n = 7$  and  $l = 5$ , where  $n$  and  $l$  are the principal and orbital quantum numbers, respectively. Both the calculations, however, include the core polarization contribution from  $2s$  and  $2p$  electrons only. The revised result, 23.11, from Ref. [13] is larger by about 12% than the experiment. Our result, 20.20, is smaller by about 14% than Ref. [13], and hence in good agreement with experiment. In our calculation, the active space includes orbitals up to  $n = 25$  and  $l = 5$ , with CSFs arising from *core-to-valence*, *valence-to-virtuals* and *core-to-virtuals single* and *double* electron replacements to all order.

## VI. THEORETICAL UNCERTAINTY

The theoretical uncertainty in the calculated life time of  $^3P_0^o$  state will have three important contributions. These are, the uncertainties in the energy denominators  $\Delta E_{^3P_1^o}$  and  $\Delta E_{^1P_1^o}$ , the hyperfine reduced matrix elements  $\langle ^3P_1^o || t^1 || ^3P_0^o \rangle$  and  $\langle ^1P_1^o || t^1 || ^3P_0^o \rangle$ , and the dipole reduced

TABLE VII. Wavelength ( $\lambda$ ) (in nm), E1HFS amplitude (in a.u.) of  $^1S_0 - ^3P_0^o$  transition and the life time ( $\tau$ ) (in sec.) of  $^3P_0^o$  metastable state. Here,  $[x]$  represents  $10^x$ .

Methods	$\lambda$	E1HFS	$\tau$
CCSD	267.44	5.153[−5]	21.325
CCSD(T)		5.316[−5]	20.036
CCSD(T)+Breit+QED		5.295[−5]	20.200
Other cal.			23.11 <sup>a</sup> , 20.33 <sup>b</sup>
Exp.	267.43		20.6 ± 1.4 <sup>c</sup>

<sup>a</sup> Ref.[13][MCDF], <sup>b</sup> Ref.[12][MCDF], <sup>c</sup> Ref.[5]

matrix elements  $\langle ^1S_0 || d || ^3P_1^o \rangle$  and  $\langle ^1S_0 || d || ^1P_1^o \rangle$ . The uncertainties in  $\Delta E_{^3P_1^o}$  and  $\Delta E_{^1P_1^o}$  are calculated using the relative errors in the excitation energies of  $^3P_0^o$ ,  $^3P_1^o$  and  $^1P_1^o$  states given in Table II, and these are  $\approx 0.01\%$  and  $0.43\%$ , respectively. As there are no experimental results for hyperfine constants and there is large variation in the experimental data for oscillator strengths, we have identified four different sources which can contribute to the uncertainty in the above dipole and hyperfine reduced matrix elements. The first source of uncertainty is due to the truncation of the basis set in our calculation. As discussed in the basis convergence subsection, our calculated values of hyperfine structure constants and E1 transition amplitudes converge to the order of  $10^{-3}$  or more as the function of basis sets. Since the change is very small, we can neglect this uncertainty. The second source of uncertainty is due to the truncation of the dressed Hamiltonian  $\hat{H}_{\text{hfs}}^e$  to the second order in  $T^{(0)}$ . In our previous work on hyperfine structure constants [25], using an iterative scheme, we have shown that the contribution from the third and higher order terms in  $T^{(0)}$  is less than 0.1%. So, we consider 0.1% as an upper bound for this source of uncertainty. The third source of uncertainty is due to the partial inclusion of the triple excitations in the properties calculations. Since perturbative triples account for the leading order contribution, we use the contributions from them as the upper bound [45, 46]. The fourth source of uncertainty is associated with the frequency-dependent Breit interaction which we do not include in the present work. However, in our previous work [45] using a series of computations with GRASP2K which implements this interaction we estimated an upper bound on this uncertainty to be 0.13% in Ra. Although Al<sup>+</sup> is much lighter atom and expected to have much smaller contribution from frequency-

dependent Breit interaction, we take 0.13% as an upper bound from this source. There could be other sources of theoretical uncertainty, such as the higher order coupled perturbation of vacuum polarization and self-energy terms, quadruply excited cluster operators, etc. But, these, in general, have much lower contributions to the properties and their cumulative theoretical uncertainty could be below 0.1%. By combining the upper bounds from all sources of uncertainties, we obtain the theoretical uncertainty in our calculated life time of the  ${}^3P_0^o$  state below 3.4%.

## VII. CONCLUSIONS

We have developed an all particle Fock-space relativistic coupled-cluster based method for properties calculation of two-valence atomic systems. To account for the relativistic effects and QED corrections we have implemented the Dirac-Coulomb-Breit Hamiltonian with the corrections from the Uehling potential and the self-energy. The effects of triple excitations are incorporated using the perturbative triples approach. Using method we have calculated the properties such as the excitation energies, hyperfine structure constants and reduced matrix elements, oscillator strengths and the life time associated with  ${}^1S_0 - {}^3P_0^o$  clock transition in  $\text{Al}^+$ . Our results

on excitation energies and oscillator strengths agrees well with the available experimental data. The calculated life time of  ${}^3P_0^o$  metastable state,  $20.20 \pm 0.68$  s, is in excellent agreement with the experimental value,  $20.60 \pm 1.4$  s, from Rosenband *et al.* [5]. From our calculations we also found that the contributions from the triple excitations and Breit+QED corrections are critical to obtain the accurate clock properties in  $\text{Al}^+$ . Based on our analysis, the upper bound on the theoretical uncertainty in the calculated life time of  ${}^3P_0^o$  is 3.4%. Such an accuracy of our result indicates that the FSRCC method we have developed has the potential to predict the clock and other atomic properties with an accuracy commensurate with the atomic experiments.

## ACKNOWLEDGMENTS

We would like to thank B P Das for useful suggestions on the manuscript. We also thank Chandan Kumar Vishwakarma for valuable discussions. One of the authors, BKM, acknowledges the funding support from the SERB (ECR/2016/001454). The results presented in the paper are based on the computations using the High Performance Computing cluster, Padum, at the Indian Institute of Technology Delhi, New Delhi.

---

[1] S. G. Karshenboim and E Peik, *Astrophysics, Clocks and Fundamental Constants, Lecture Notes in Physics* (Springer, New York, 2010).

[2] M. S. Grewal, A. P. Andrews, and C. G. Bartone, *Global Navigation Satellite Systems, Inertial Navigation, and Integration* (John Wiley and Sons, New York, 2013).

[3] M. S. Safronova, D. Budker, D. DeMille, Derek F. Jackson Kimball, A. Derevianko, and Charles W. Clark, “Search for new physics with atoms and molecules,” *Rev. Mod. Phys.* **90**, 025008 (2018).

[4] Fritz Riehle, Patrick Gill, Felicitas Arias, and Lennart Robertsson, “The CIPM list of recommended frequency standard values: guidelines and procedures,” *Metrologia* **55**, 188–200 (2018).

[5] T. Rosenband, P. O. Schmidt, D. B. Hume, W. M. Itano, T. M. Fortier, J. E. Stalnaker, K. Kim, S. A. Diddams, J. C. J. Koelemeij, J. C. Bergquist, and D. J. Wineland, “Observation of the  ${}^1S_0 \rightarrow {}^3P_0$  clock transition in  ${}^{27}\text{Al}^+$ ,” *Phys. Rev. Lett.* **98**, 220801 (2007).

[6] C. W. Chou, D. B. Hume, J. C. J. Koelemeij, D. J. Wineland, and T. Rosenband, “Frequency comparison of two high-accuracy  $\text{Al}^+$  optical clocks,” *Phys. Rev. Lett.* **104**, 070802 (2010).

[7] J.-S. Chen, S. M. Brewer, C. W. Chou, D. J. Wineland, D. R. Leibrandt, and D. B. Hume, “Sympathetic ground state cooling and time-dilation shifts in an  ${}^{27}\text{Al}^+$  optical clock,” *Phys. Rev. Lett.* **118**, 053002 (2017).

[8] S. M. Brewer, J.-S. Chen, A. M. Hankin, E. R. Clements, C. W. Chou, D. J. Wineland, D. B. Hume, and D. R. Leibrandt, “ ${}^{27}\text{Al}^+$  quantum-logic clock with a systematic uncertainty below  $10^{-18}$ ,” *Phys. Rev. Lett.* **123**, 033201 (2019).

[9] S. M. Brewer, J.-S. Chen, K. Beloy, A. M. Hankin, E. R. Clements, C. W. Chou, W. F. McGrew, X. Zhang, R. J. Fasano, D. Nicolodi, H. Leopardi, T. M. Fortier, S. A. Diddams, A. D. Ludlow, D. J. Wineland, D. R. Leibrandt, and D. B. Hume, “Measurements of  ${}^{27}\text{Al}^+$  and  ${}^{25}\text{Mg}^+$  magnetic constants for improved ion-clock accuracy,” *Phys. Rev. A* **100**, 013409 (2019).

[10] Mihály Kállay, H. S. Nataraj, B. K. Sahoo, B. P. Das, and Lucas Visscher, “Relativistic general-order coupled-cluster method for high-precision calculations: Application to the  $\text{Al}^+$  atomic clock,” *Phys. Rev. A* **83**, 030503 (2011).

[11] M. S. Safronova, M. G. Kozlov, and Charles W. Clark, “Precision Calculation of Blackbody Radiation Shifts for Optical Frequency Metrology,” *Phys. Rev. Lett.* **107**, 143006 (2011).

[12] Tomas Brage, Philip G. Judge, Abdellatif Aboussaid, Michel R. Godefroid, Per Jonsson, Anders Ynnerman, Char lotte Froese Fischer, and David S. Leckrone, “Hyperfine Induced Transitions as Diagnostics of Isotopic Composition and Densities of Low-Density Plasmas,” *The Astrophysical Journal* **500**, 507–521 (1998).

[13] Huihui Kang, Jiguang Li, Chenzhong Dong, Per Jonsson, and Gediminas Gaigalas, “Hyperfine quenching of the  ${}^3s3p$   ${}^3P_0$  level in Mg-like ions,” *J. Phys. B: At. Mol. Opt. Phys.* **42**, 195002 (2009).

[14] R. Pal, M. S. Safronova, W. R. Johnson, A. Derevianko, and S. G. Porsev, “Relativistic coupled-cluster single-double method applied to alkali-metal atoms,” *Phys. Rev. A* **75**, 042515 (2007).

[15] B. K. Mani, K. V. P. Latha, and D. Angom, “Relativistic coupled-cluster calculations of  ${}^{20}\text{Ne}$ ,  ${}^{40}\text{Ar}$ ,  ${}^{84}\text{Kr}$ , and  ${}^{129}\text{Xe}$ : Correlation energies and dipole polarizabilities,” *Phys. Rev. A* **80**, 062505 (2009).

[16] H. S. Nataraj, B. K. Sahoo, B. P. Das, and D. Mukherjee, “Reappraisal of the electric dipole moment enhancement factor for thallium,” *Phys. Rev. Lett.* **106**, 200403 (2011).

[17] Ravi Kumar, S. Chattopadhyay, B. K. Mani, and D. Angom, “Electric dipole polarizability of group-13 ions using perturbed relativistic coupled-cluster theory: Importance of non-linear terms,” *Phys. Rev. A* **101**, 012503 (2020).

[18] Ephraim Eliav, Uzi Kaldor, and Yasuyuki Ishikawa, “Transition energies of ytterbium, lutetium, and lawrencium by the relativistic coupled-cluster method,” *Phys. Rev. A* **52**, 291–296 (1995).

[19] Ephraim Eliav, Uzi Kaldor, and Yasuyuki Ishikawa, “Transition energies of mercury and ekamercury (element 112) by the relativistic coupled-cluster method,” *Phys. Rev. A* **52**, 2765–2769 (1995).

[20] B. K. Mani and D. Angom, “Fock-space relativistic coupled-cluster calculations of two-valence atoms,” *Phys. Rev. A* **83**, 012501 (2011).

[21] A. K. Mohanty, F. A. Parpia, and E. Clementi, “Kinetically balanced geometric gaussian basis set calculations for relativistic many-electron atoms,” in *Modern Techniques in Computational Chemistry: MOTECC-91*, edited by E. Clementi (ESCOM, 1991).

[22] Richard E. Stanton and Stephen Havriliak, “Kinetic balance: A partial solution to the problem of variational safety in dirac calculations,” *J. Chem. Phys.* **81**, 1910–1918 (1984).

[23] Debasish Mukherjee, “The linked-cluster theorem in the open-shell coupled-cluster theory for incomplete model spaces,” *Chemical Physics Letters* **125**, 207 – 212 (1986).

[24] W.R. Johnson, *Atomic Structure Theory: Lectures on Atomic Physics* (Springer, Berlin, 2007).

[25] B. K. Mani and D. Angom, “Atomic properties calculated by relativistic coupled-cluster theory without truncation: Hyperfine constants of Mg<sup>+</sup>, Ca<sup>+</sup>, Sr<sup>+</sup>, and Ba<sup>+</sup>,” *Phys. Rev. A* **81**, 042514 (2010).

[26] I. Lindgren and J. Morrison, *Atomic Many-Body Theory* (Springer, Berlin, 2nd Edition, 1986).

[27] P. Jönsson, G. Gaigalas, J. Bieroń, C. Froese Fischer, and I. P. Grant, “New version: Grasp2k relativistic atomic structure package,” *Comp. Phys. Comm.* **184**, 2197 – 2203 (2013).

[28] “Nist atomic spectroscopic database,” <https://physics.nist.gov/PhysRefData/ASD/levels.html> (2013).

[29] E. A. Konovalova and M. G. Kozlov, “Correlation, Breit, and QED effects in spectra of Mg-like ions,” *Phys. Rev. A* **92**, 042508 (2015).

[30] Mitroy, J., Zhang, J. Y., Bromley, M. W.J., and Rollin, K. G., “Blackbody radiation shift of the Al<sup>+</sup> clock transition,” *Eur. Phys. J. D* **53**, 15–19 (2009).

[31] M Stanek, L Glowacki, and J Migdalek, “The spin-allowed and spin-forbidden  $3s^2 \ ^1S_0 - 3s3p \ ^1P_1, ^3P_1$  transitions in the magnesium isoelectronic sequence,” *J. Phys. B: At. Mol. Opt. Phys.* **29**, 2985–2996 (1996).

[32] B. P. Das and M. Idrees, “Some theoretical aspects of the group-III A-ion atomic clocks: Intercombination transition probabilities,” *Phys. Rev. A* **42**, 6900–6902 (1990).

[33] Hsiang-Shun Chou, Hsin-Chang Chi, and Keh-Ning Huang, “Relativistic excitation energies and oscillator strengths including core-polarization effects for the intercombination and resonance transitions in Mg-like ions,” *J. Phys. B: At. Mol. Opt. Phys.* **26**, 4079–4089 (1993).

[34] Yu Zou and C. Froese Fischer, “Multiconfiguration Dirac-Hartree-Fock optimization strategies for  $3s^2 \ ^1S_0 - 3s3p \ ^3P_1$  transition rates for Al<sup>+</sup>– S<sup>4+</sup>,” *Phys. Rev. A* **62**, 062505 (2000).

[35] U. I. Safranova, W. R. Johnson, and H. G. Berry, “Excitation energies and transition rates in magnesiumlike ions,” *Phys. Rev. A* **61**, 052503 (2000).

[36] P. Jonsson and C. Froese Fischer, “Accurate multi-configuration Dirac - Fock calculations of transition probabilities in the Mg isoelectronic sequence,” *J. Phys. B: At. Mol. Opt. Phys.* **30**, 5861–5875 (1997).

[37] W R Johnson, M S Safranova, and U I Safranova, “Relativistic many-body calculations of energies of Mg I, Al II, Al I, Hg I, Tl II, Tl I, Pb I, Bi II and Bi I,” *Physica Scripta* **56**, 252–263 (1997).

[38] W. M. Itano, J. C. Bergquist, A. Brusch, S. A. Diddams, T. M. Fortier, T. P. Heavner, L. Hollberg, D. B. Hume, S. R. Jefferts, L. Lorini, T. E. Parker, T. Rosenband, and J. E. Stalnaker, “Optical frequency standards based on mercury and aluminum ions,” in *Time and Frequency Metrology*, Vol. 6673, edited by R. Jason Jones, International Society for Optics and Photonics (Proc. of SPIE, 2007) pp. 9 – 19.

[39] K. Beloy, D. R. Leibrandt, and W. M. Itano, “Hyperfine-mediated electric quadrupole shifts in Al<sup>+</sup> and In<sup>+</sup> ion clocks,” *Phys. Rev. A* **95**, 043405 (2017).

[40] B. C. Johnson, P. L. Smith, and W. H. Parkinson, “Transition probability of the AL II 2669 intersystem line,” *Astrophys. J.* **308**, 1013–1017 (1986).

[41] J A Kernahan, E H Pinnington, J A O Neill, R L Brooks, and K E Donnelly, “Radiative lifetime measurements in Al II-VII,” *Physica Scripta* **19**, 267–270 (1979).

[42] Baudinet-Robinet, Y., Dumont, P. D., Garnir, H. P., Biémont, E., and Grevesse, N., “Beam-foil study of Al II-VI between 1110 and 1900 Å,” *J. Phys. Colloques* **40**, C1–175–C1–179 (1979).

[43] H G Berry, J Bromander, and R Buchta, “Some mean life measurements in the Na I and Mg I isoelectronic sequences,” *Physica Scripta* **1**, 181–183 (1970).

[44] P. Shorer, C. D. Lin, and W. R. Johnson, “Oscillator strengths for the magnesium isoelectronic sequence,” *Phys. Rev. A* **16**, 1109–1116 (1977).

[45] S. Chattopadhyay, B. K. Mani, and D. Angom, “Electric dipole polarizability of alkaline-earth-metal atoms from perturbed relativistic coupled-cluster theory with triples,” *Phys. Rev. A* **89**, 022506 (2014).

[46] S. Chattopadhyay, B. K. Mani, and D. Angom, “Electric dipole polarizabilities of doubly ionized alkaline-earth-metal ions from perturbed relativistic coupled-cluster theory,” *Phys. Rev. A* **87**, 062504 (2013).